JOURNAL OF GUIDANCE, CONTROL, AND DYNAMICS
Vol. 25, No. 2, March–April 2002

Nonlinear Tracking Control for Satellite Formations

Hsi-Han Yeh,* Eric Nelson,† and Andrew Sparks‡
U.S. Air Force Research Laboratory, Wright–Patterson Air Force Base, Ohio 45433-7521

A tracking control design using sliding mode techniques is derived to control a desired satellite formation. Hill's relative motion equations are used to model the follower satellite motion relative to the leader. To minimize fuel usage required to maintain the formation, each satellite is constrained to reside near a natural orbit. Control forces are applied only to maintain the desired relative motion by correcting for initial offsets and perturbation effects that tend to disperse the formation. These perturbations include effects due to Earth asphericity, atmospheric drag, and third-body effects from the sun and moon. Parametric equations describing the member satellites' relative motion with respect to the leader satellite are essential in this design. The control law is modified to account for discontinuous nature of the control forces available with the satellite propulsive thrusters. Numerical simulations using a high-fidelity, nonlinear model demonstrate the control law performance for the full nonlinear dynamics with high-order perturbations.

I. Introduction

SATELLITE formations are subject to different constraints than ground or air vehicle formations. Because of fuel capacity limitations, each satellite in a formation must reside near a natural orbit. Fuel is expended only to correct the initial deployment inaccuracy and to overcome the perturbation effects that tend to dislodge the satellite from the desired orbit. These perturbations include the effects of Earth oblateness, atmospheric drag, and solar and lunar gravity.[1] Among these perturbations, the most significant is the second spherical harmonic in the Earth's gravity field due to oblateness (known as the J_2 effect). The J_2 effect causes an uncontrolled formation to disperse.[2]

Recently, Schaub et al.[3] designed a formation control law based on Gauss's variational equations of motion for a satellite to track its assigned J_2 invariant orbit (see Ref. 4). This approach describes an overdetermined system, that is, more output variables than inputs. The control vector is determined through a least-square solution. Therefore, the resulting control law does not guarantee a stable system. Numerical simulation in Ref. 3 does show that the control law maintains the satellite's desired orbit.

This paper shows a tracking control design that forms the desired satellite formation after the initial deployment and nudges the members back into formation when they drift from the desired dynamics. Instead of Gauss's variational equations of motions, we use Hill's (or Clohessy–Wiltshire) equations to model the follower satellite relative motion with respect to the leader. Hill's equations are a first-order approximation that describe the follower satellite relative motion around a leader in a circular orbit. The satellites are orbiting around a spherical Earth. In Hill's equations or the complete nonlinear dynamic equations, the control variables are uniquely determined by a given output set. In mathematical language, the input and output manifolds are diffeomorphic. Thus, the tracking control avoids control variable overdetermination and guarantees system stability.

II. Sliding Mode Control

This section considers the theoretical basis for incorporating a multiple satellite formation control problem into the sliding mode framework. The control problem is formulated using state feedback. Although this is a limitation in general, in the case of the satellite formation control problem this assumption does not present a problem because all of the states are available for feedback through differential carrier-phase global positioning system.

A. Relative Degree

Consider a nonlinear dynamic system of the form

$$\dot{\boldsymbol{x}}(t) = \boldsymbol{f}(\boldsymbol{x}, t) + \boldsymbol{G}(\boldsymbol{x}, t)\boldsymbol{u}(t), \qquad \boldsymbol{y}(t) = \boldsymbol{h}(\boldsymbol{x}, t) = \begin{bmatrix} \boldsymbol{h}_1(\boldsymbol{x}, t) \\ \vdots \\ \boldsymbol{h}_m(\boldsymbol{x}, t) \end{bmatrix} \tag{1}$$

where $\boldsymbol{x}(t)$, $\boldsymbol{u}(t)$, and $\boldsymbol{y}(t)$ are n-, m-, and m-dimensional real vectors, $\boldsymbol{f}(\boldsymbol{x}, t)$, $\boldsymbol{G}(\boldsymbol{x}, t)$, and $\boldsymbol{h}(\boldsymbol{x}, t)$ are analytic vector or matrix functions of the variables $\boldsymbol{x}$ and t. We need an operator to give output time derivatives when the system is free from the control input. Define the operator L_f as

$$L_f \boldsymbol{h}_i(\boldsymbol{x}, t) := \frac{\mathrm{d}}{\mathrm{d}t}\boldsymbol{h}_i(\boldsymbol{x}, t)|_{u=0} = \frac{\partial}{\partial t}\boldsymbol{h}_i(\boldsymbol{x}, t) + \frac{\partial \boldsymbol{h}_i(\boldsymbol{x}, t)}{\partial \boldsymbol{x}}\boldsymbol{f}(\boldsymbol{x}, t) \qquad i = 1, \ldots, m$$

$$L_f^j \boldsymbol{h}_i(\boldsymbol{x}, t) := L_f\left[L_f^{j-1}\boldsymbol{h}_i(\boldsymbol{x}, t)\right], \qquad j \geq 1$$

$$L_f^0 \boldsymbol{h}_i(\boldsymbol{x}, t) := \boldsymbol{h}_i(\boldsymbol{x}, t) \tag{2}$$

Thus, $L_f^j \boldsymbol{h}_i(\boldsymbol{x}, t)$ is the jth time derivative of $\boldsymbol{h}_i(\boldsymbol{x}, t)$ when $\boldsymbol{u} = 0$. Similarly, we define

$$L_G \boldsymbol{h}_i(\boldsymbol{x}, t) := \frac{\partial \boldsymbol{h}_i(\boldsymbol{x}, t)}{\partial \boldsymbol{x}}\boldsymbol{G}(\boldsymbol{x}, t) \tag{3}$$

Notice that $\boldsymbol{h}_i(x, t)$ might not couple directly with the control variable $\boldsymbol{u}$, but some $\boldsymbol{h}_i(\boldsymbol{x}, t)$ time derivatives are coupled to $\boldsymbol{u}$. Let α_i be the lowest-order $\boldsymbol{h}_i(\boldsymbol{x}, t)$ time derivative that is coupled to $\boldsymbol{u}$. That is,

$$\alpha_i := \min\left\{j \mid L_G L_f^{j-1}\boldsymbol{h}_i(\boldsymbol{x}, t) \neq 0\right\}, \qquad i = 1, 2, \ldots, m \tag{4}$$

Note that implicitly in the definition of Eq. (4) $\alpha_i \geq 1$. We interpret $\alpha_i = 0$ to mean that the ith output variable is directly connected to the control variable. However, this does not happen in most dynamic control systems, including this satellite application. Henceforth in this paper, we shall assume that the outputs are not directly coupled to the control variables and will always have $\alpha_i \geq 1$.

If we differentiate $\boldsymbol{h}_i(\boldsymbol{x}, t)$ until $\boldsymbol{u}(t)$ appears in its expression, the highest $\boldsymbol{h}_i(\boldsymbol{x}, t)$ derivative will have an order of α_i. That is,

$$\boldsymbol{y}_i^{(j)}(t) = L_f^j \boldsymbol{h}_i(\boldsymbol{x}, t), \qquad j = 0, 1, \ldots, \alpha_i - 1$$

$$\boldsymbol{y}_i^{(\alpha_i)}(t) = L_f^{\alpha_i}\boldsymbol{h}_i(\boldsymbol{x}, t) + L_G L_f^{\alpha_i - 1}\boldsymbol{h}_i(\boldsymbol{x}, t)\boldsymbol{u}(t) \tag{5}$$

Received 12 September 2000; revision received 21 May 2001; accepted for publication 11 June 2001.

*Electronics Engineer, Control Theory Optimization Branch.
†Stability and Control Engineer, Control Theory Optimization Branch. Member AIAA.
‡Senior Aerospace Engineer, Control Theory Optimization Branch. Senior Member AIAA.

Now define

$$\boldsymbol{y}^{(\alpha)}(t) := \begin{bmatrix} \boldsymbol{y}_1^{(\alpha_1)} \\ \boldsymbol{y}_2^{(\alpha_2)} \\ \vdots \\ \boldsymbol{y}_m^{(\alpha_m)} \end{bmatrix} \tag{6}$$

Then,

$$\boldsymbol{y}^{(\alpha)}(t) = \boldsymbol{a}^*(\boldsymbol{x}, t) + \boldsymbol{B}^*(\boldsymbol{x}, t)\boldsymbol{u}(t) \tag{7}$$

where $B^*(x, t)$ is the matrix through which control $\boldsymbol{u}(t)$ is coupled to the $h(x, t)$ component's lowest derivative and

$$\boldsymbol{a}^*(\boldsymbol{x}, t) := \begin{bmatrix} L_f^{\alpha_1}\boldsymbol{h}_1(\boldsymbol{x}, t) \\ \vdots \\ L_f^{\alpha_m}\boldsymbol{h}_m(\boldsymbol{x}, t) \end{bmatrix}$$

$$\boldsymbol{B}^*(\boldsymbol{x}, t) := \begin{bmatrix} L_G L_f^{\alpha_1 - 1}\boldsymbol{h}_1(\boldsymbol{x}, t) \\ \vdots \\ L_G L_f^{\alpha_m - 1}\boldsymbol{h}_m(\boldsymbol{x}, t) \end{bmatrix} \tag{8}$$

Because system (1) has the same number of controls as outputs, $\boldsymbol{B}^*(\boldsymbol{x}, t)$ is a square matrix. If $\boldsymbol{B}^*(\boldsymbol{x}, t)$ is nonsingular at a point x_0, then the vector $(\alpha_1, \alpha_2, \ldots, \alpha_m)$ is called the relative degree of the system (1) at that point. We shall assume that $\boldsymbol{B}^*(\boldsymbol{x}, t)$ is nonsingular at some operating point $\boldsymbol{x}_0$. We shall refer to $\boldsymbol{y}^{(\alpha)}(t)$ as the derivative of $\boldsymbol{y}(t)$ to the relative degree of the plant.[5]

B. Relay Control Design

For a multi-input/multi-output system, the relative degree vector provides insight to sliding plane selection in a sliding mode control design. In this section, we define the sliding plane in terms of the error from the reference trajectory, then derive the sliding mode control law to stabilize the system and provide tracking along the reference trajectory.

The reference trajectory is represented by $\hat{\boldsymbol{y}}(t)$, and the tracking error is defined as

$$\boldsymbol{e}(t) := \hat{\boldsymbol{y}}(t) - \boldsymbol{y}(t) = \begin{bmatrix} \boldsymbol{e}_1(t) \\ \boldsymbol{e}_2(t) \\ \vdots \\ \boldsymbol{e}_m(t) \end{bmatrix} \tag{9}$$

For each output y_i, define a sliding plane of the form

$$\sigma_i[\boldsymbol{e}_i(t)] = k_{\alpha_i}^i \boldsymbol{e}^{(\alpha_i - 1)}(t) + k_{\alpha_i - 1}^i \boldsymbol{e}^{(\alpha_i - 2)}(t) + \cdots + k_1^i \boldsymbol{e}(t) + k_0^i \boldsymbol{e}_s(t) + k_s^i \boldsymbol{e}_{ss}(t) \tag{10}$$

Written in vector form,

$$\sigma[\boldsymbol{e}(t)] = \begin{bmatrix} \sigma_1[\boldsymbol{e}_1(t)] \\ \sigma_2[\boldsymbol{e}_2(t)] \\ \vdots \\ \sigma_m[\boldsymbol{e}_m(t)] \end{bmatrix} = K_\alpha \boldsymbol{e}^{(\alpha - 1)}(t) + K_{\alpha - 1}\boldsymbol{e}^{(\alpha - 2)}(t) + \cdots + K_1 \boldsymbol{e}(t) + K_0 \boldsymbol{e}_s(t) + K_s \boldsymbol{e}_{ss}(t) \tag{11}$$

where

$$\boldsymbol{e}^{(\alpha)}(t) = \begin{bmatrix} \boldsymbol{e}_1^{(\alpha_1)}(t) \\ \boldsymbol{e}_2^{(\alpha_2)}(t) \\ \vdots \\ \boldsymbol{e}_m^{(\alpha_m)}(t) \end{bmatrix}$$

$$\boldsymbol{e}_s(t) = \int \boldsymbol{e}(t)\, \mathrm{d}t, \qquad \int \boldsymbol{e}_s(t)\, \mathrm{d}t = \boldsymbol{e}_{ss}(t)$$

and where $K_{\alpha - j}$ are diagonal matrices with elements $k_{\alpha - j}^i$, whose elements may be zero depending on the relative degree vector. In addition, the highest nonzero $k_{\alpha - j}^i$ can be arbitrarily set to one without loss of generality. For example, suppose a system having two outputs has relative degree vector (3, 2). The matrices $K_{\alpha - j}$ would be defined as $K_3 = \mathrm{diag}(1, 0)$, $K_2 = \mathrm{diag}(k_2^1, 1)$, $K_1 = \mathrm{diag}(k_1^1, k_1^2)$ to account for a sliding plane for the first output having a $\boldsymbol{e}^{(2)}(t)$ term and one for the second output having a $\boldsymbol{e}^{(1)}(t)$ term.

Because the highest-order derivative in Eq. (11) is lower than the relative degree of the plant by exactly one, the right-hand side of Eq. (11) does not involve the control vector $\boldsymbol{u}(t)$. Instead, $\dot{\sigma}(\boldsymbol{e})$ will contain $\boldsymbol{u}(t)$. This makes the sliding mode control solution easy to obtain when a quadratic function $\sigma(\boldsymbol{e})$ is used as the Lyapunov function. On the other hand, if the sliding plane is of equal or higher order than the relative degree, the sliding mode control solution becomes unwieldy. If the sliding plane is of lower order than the plant's relative degree by more than one, $\dot{\sigma}(\boldsymbol{e})$ will not explicitly depend on $\boldsymbol{u}(t)$, and no sliding mode exists on $\sigma(\boldsymbol{e}) = 0$. In this fashion, the relative degree vector dictates the sliding plane selection that is linear in the error signal.

We shall design an on–off sliding mode controller that keeps the plant state (1) on the sliding plane Eq. (11). We select a candidate Lyapunov function as follows:

$$V = \tfrac{1}{2}\sigma^T(\boldsymbol{e})\sigma(\boldsymbol{e}) \tag{12}$$

The derivative of V is

$$\dot{V} = \sigma^T(\boldsymbol{e})\dot{\sigma}(\boldsymbol{e}) \tag{13}$$

Differentiating Eq. (11) with the aid of Eqs. (7) and (9) yields

$$\dot{\sigma}(\boldsymbol{e}) = \tilde{\boldsymbol{u}}(t) - \boldsymbol{B}^*(\boldsymbol{x}, t)\boldsymbol{u}(t) \tag{14}$$

where

$$\tilde{\boldsymbol{u}}(t) = \hat{\boldsymbol{y}}^{(\alpha)}(t) + K_{\alpha - 1}\boldsymbol{e}^{(\alpha - 1)}(t) + \cdots + K_0 \boldsymbol{e}(t) + K_s \boldsymbol{e}_s(t) - \boldsymbol{a}^*(\boldsymbol{x}, t) \tag{15}$$

Substituting Eq. (14) into Eq. (13) gives

$$\begin{aligned} \dot{V} &= \sigma^T(\boldsymbol{e})[\tilde{\boldsymbol{u}}(t) - \boldsymbol{B}^*(\boldsymbol{x}, t)\boldsymbol{u}(t)] \\ &= \sigma^T(\boldsymbol{e})\boldsymbol{B}^*(\boldsymbol{x}, t)[\boldsymbol{B}^{*-1}(\boldsymbol{x}, t)\tilde{\boldsymbol{u}}(t) - \boldsymbol{u}(t)] \end{aligned} \tag{16}$$

Sliding mode control design finds $\boldsymbol{u}(t)$ such that $\sigma^T(\boldsymbol{e})\dot{\sigma}(\boldsymbol{e})$ is always negative. There are many ways to achieve this goal. One solution can take the following form:

$$\boldsymbol{u}(t) = \boldsymbol{B}^{*-1}(\boldsymbol{x}, t)\tilde{\boldsymbol{u}}(t) + \boldsymbol{u}_a(t) \tag{17}$$

with

$$\boldsymbol{u}_a(t) = \begin{cases} \rho\, \mathrm{sgn}[\boldsymbol{B}^{*T}(\boldsymbol{x}, t)\sigma(\boldsymbol{e})], & \rho > 0, \quad \sigma(\boldsymbol{e}) \neq 0 \\ 0, & \sigma(\boldsymbol{e}) = 0 \end{cases} \tag{18}$$

where ρ is defined as a diagonal matrix,

$$\rho := \mathrm{diag}(\rho_1, \rho_2, \ldots, \rho_m) \tag{19}$$

and the vector signum function is a column of signum function:

$$\mathrm{sgn}\,\sigma(\boldsymbol{e}) = [\mathrm{sgn}\sigma_1(\boldsymbol{e}) \quad \mathrm{sgn}\sigma_2(\boldsymbol{e}) \quad \cdots \quad \mathrm{sgn}\sigma_m(\boldsymbol{e})]^T \tag{20}$$

The control law (17) drives the system to the sliding plane. The control vector that sets $\dot{\sigma}(\boldsymbol{e})$ to zero is described as the equivalent control.[6] The sliding plane equivalent control (11) is the continuous component of Eq. (17) [with $\boldsymbol{u}_a(t) = 0$]. Because this equivalent control forces the system to stay on a linear sliding plane, the equivalent control is also labeled as a feedback linearizing control. If the sliding plane Eq. (11) is chosen with dynamics that quickly reduce the error signal, then the closed-loop system will have good performance.

The equivalent control, as shown in Eq. (17), is difficult to implement for satellite control systems. Although the thruster pulse

widths are adjustable, the thrust magnitudes are not. To implement a discontinuous sliding mode control design without the continuous component, let

$$\boldsymbol{u}(t) = \rho \operatorname{sgn}[\boldsymbol{B}^{*T}(\boldsymbol{x}, t)\sigma(\boldsymbol{e})], \qquad \rho_i > \max\left|\boldsymbol{B}_i^{*-1}(\boldsymbol{x}, t)\tilde{\boldsymbol{u}}(t)\right| \quad i = 1, 2, \ldots, m \tag{21}$$

where $\boldsymbol{B}_i^{*-1}(\boldsymbol{x}, t)$ is the ith row of $\boldsymbol{B}^{*-1}(\boldsymbol{x}, t)$. The control law in Eq. (21) gives an asymptotically stable closed-loop system, as shown by substituting Eq. (21) into Eq. (16):

$$\begin{aligned}\dot{V} &= \sigma^T(\boldsymbol{e})\boldsymbol{B}^*(\boldsymbol{x}, t)\{\boldsymbol{B}^{*-1}(\boldsymbol{x}, t)\tilde{\boldsymbol{u}}(t) - \rho \operatorname{sgn}[\boldsymbol{B}^{*T}(\boldsymbol{x}, t)\sigma(\boldsymbol{e})]\} \\ &= \sigma^T(\boldsymbol{e})\boldsymbol{B}^*(\boldsymbol{x}, t)\{-\tilde{\rho}(t) \operatorname{sgn}[\boldsymbol{B}^{*T}(\boldsymbol{x}, t)\sigma(\boldsymbol{e})]\}\end{aligned} \tag{22}$$

where

$$\tilde{\rho}_i(t) = \begin{cases} \rho_i + \boldsymbol{B}_i^{*-1}(\boldsymbol{x}, t)\tilde{\boldsymbol{u}}(t), & \text{if } \left[\boldsymbol{B}_i^T(\boldsymbol{x}, t)\sigma(\boldsymbol{e})\right] < 0 \\ \rho_i - \boldsymbol{B}_i^{*-1}(\boldsymbol{x}, t)\tilde{\boldsymbol{u}}(t), & \text{if } \left[\boldsymbol{B}_i^T(\boldsymbol{x}, t)\sigma(\boldsymbol{e})\right] > 0 \end{cases} \tag{23}$$

for $i = 1, 2, \ldots, m$. Because ρ_i is sufficiently large, $\tilde{\rho}_i(t) > 0$. Therefore, $\dot{V}$ is always negative whenever $\sigma(\boldsymbol{e}) \neq 0$. Thus, this control law drives the system to the sliding plane Eq. (11). The control vector magnitude ρ [Eq. (21)] is typically selected to reflect the application and is easily adjusted to accommodate a changing control problem.

The control law of Eq. (21) can also drive any finite initial state to the sliding plane in finite time. To see this, we rearrange Eq. (22) to give

$$\begin{aligned}\dot{V} &= \sigma^T(\boldsymbol{e})\boldsymbol{B}^*(\boldsymbol{x}, t)\{-\tilde{\rho}(t) \operatorname{sgn}[\boldsymbol{B}^{*T}(\boldsymbol{x}, t)\sigma(\boldsymbol{e})]\} \\ &\leq -\rho'|\sigma^T(\boldsymbol{e})\boldsymbol{B}^*(\boldsymbol{x}, t)| \leq -\rho'' V^{\frac{1}{2}}, \qquad \rho', \rho'' > 0\end{aligned} \tag{24}$$

Since $V > 0$, multiplying Eq. (24) by $\frac{1}{2}V^{-1/2}$ produces

$$\tfrac{1}{2}V^{-\frac{1}{2}}\dot{V} \leq -\tfrac{1}{2}\rho'' < 0 \tag{25}$$

By integrating Eq. (25) from 0 to t, we find that

$$V^{\frac{1}{2}}(t) \leq V^{\frac{1}{2}}(0) - \tfrac{1}{2}\rho'' t \tag{26}$$

The time required for the Lyapunov function to reach zero is now defined as T. Then Eq. (26) implies

$$T \leq 2V^{\frac{1}{2}}(0) \big/ \rho'' \tag{27}$$

Thus, the Lyapunov function reaches zero in finite time. The magnitude of discontinuous control is the design parameter that determines the reaching time.

The main drawback of the sliding mode control method is that when an unstable high-frequency plant mode is excited, the discontinuous control may exhibit a chattering phenomenon. Chattering describes rapid control signal switching between positive and negative values. The most common way to avoid chattering is to introduce a boundary layer on the sliding plane.[6] Other methods include synthesizing the control variable derivatives so that the control variables themselves do not chatter.[7] In the boundary-layer approach, the discontinuous control law operates only when the system state is outside the boundary layer. Within the boundary layer, we implement a smooth transition from positive to negative, as the system state crosses the sliding plane.

The satellite control problem does not permit control force magnitude adjustments. Therefore, we cannot implement a smooth transition technique. Instead, we implement a signum function with a dead zone. Thus, Eq. (21) is modified as follows:

$$\boldsymbol{u}_i(t) = \begin{cases} \rho_i, & \text{if } \delta_i < \boldsymbol{B}_i^{*T}(\boldsymbol{x}, t)\sigma(\boldsymbol{e}) \\ 0, & \text{if } -\delta_i \leq \boldsymbol{B}_i^{*T}(\boldsymbol{x}, t)\sigma(e) \leq \delta_i \\ -\rho_i, & \text{if } \boldsymbol{B}_i^{*T}(\boldsymbol{x}, t)\sigma(\boldsymbol{e}) < -\delta_i \end{cases}$$

$$\rho_i > \max\left\|\boldsymbol{B}_i^{*-1}(\boldsymbol{x}, t)\tilde{\boldsymbol{u}}(t)\right\|, \qquad i = 1, 2, \ldots, m \tag{28}$$

for small positive values of δ_i, $i = 1, 2, \ldots, m$.

C. State Feedback Realizability

To accompany the mathmatical derivation, we can construct the feedback without taking the state derivatives. In view of Eqs. (5) and (6), the error signal derivatives in Eq. (11) are derived,

$$\begin{aligned}\dot{\boldsymbol{e}}(t) &= \dot{\hat{\boldsymbol{y}}}(t) - \dot{\boldsymbol{y}}(t) = L_{\hat{f}}\hat{\boldsymbol{h}}(\hat{\boldsymbol{x}}, t) - L_f\boldsymbol{h}(\boldsymbol{x}, t) \\ &\vdots \\ \boldsymbol{e}^{(\alpha-1)}(t) &= \hat{\boldsymbol{y}}^{(\alpha-1)}(t) - \boldsymbol{y}^{(\alpha-1)}(t) = L_{\hat{f}}^{(\alpha-1)}\hat{\boldsymbol{h}}(\hat{\boldsymbol{x}}, t) - L_f^{(\alpha-1)}\boldsymbol{h}(\boldsymbol{x}, t)\end{aligned} \tag{29}$$

where

$$L_{\hat{f}}\hat{\boldsymbol{h}}(\hat{\boldsymbol{x}}, t) = \begin{bmatrix} L_{\hat{f}}\hat{\boldsymbol{h}}_1(\hat{\boldsymbol{x}}, t) \\ \vdots \\ L_{\hat{f}}\hat{\boldsymbol{h}}_m(\hat{\boldsymbol{x}}, t) \end{bmatrix}, \qquad L_f\boldsymbol{h}(\boldsymbol{x}, t) = \begin{bmatrix} L_f\boldsymbol{h}_1(\boldsymbol{x}, t) \\ \vdots \\ L_f\boldsymbol{h}_m(\boldsymbol{x}, t) \end{bmatrix}$$

$$L_{\hat{f}}^{(\alpha-1)}\hat{\boldsymbol{h}}(\hat{\boldsymbol{x}}, t) = \begin{bmatrix} L_{\hat{f}}^{(\alpha_1-1)}\hat{\boldsymbol{h}}_1(\hat{\boldsymbol{x}}, t) \\ \vdots \\ L_{\hat{f}}^{(\alpha_m-1)}\hat{\boldsymbol{h}}_m(\hat{\boldsymbol{x}}, t) \end{bmatrix}$$

$$L_f^{(\alpha-1)}\boldsymbol{h}(\boldsymbol{x}, t) = \begin{bmatrix} L_f^{(\alpha_1-1)}\boldsymbol{h}_1(\boldsymbol{x}, t) \\ \vdots \\ L_f^{(\alpha_m-1)}\boldsymbol{h}_m(\boldsymbol{x}, t) \end{bmatrix} \tag{30}$$

Equations (29) and (30) point out that the error vector derivative of any order less than the plant's relative degree is free of the control variables. This implies that the sliding mode controls expressed in Eqs. (21) and (28) are always implementable by state feedback, without the implementation of differentiators. Differentiators can introduce unwanted high-frequency noise.

The control laws Eqs. (17), (21), and (28) all require a double integral computation, $e_{ss}(t)$, which is not a state variable of the closed-loop system. This computational burden arises from the tracking performance consideration, which requires the sliding mode equivalent control (15) to have one integration. In addition to the computational burden, the double integral also introduces phase lag. In the following designs, we shall develop sliding mode controllers using sliding plane Eq. (11) with $K_s = 0$, as well as $K_s \neq 0$, to compare their performance.

III. Satellite Control Design

In this section, we discuss the sliding plane design considerations. In addition, we present second- and third-order design examples.

A. Control Problem Formulation

We shall consider formation control using a linear model of the satellite relative dynamics to generate a reference trajectory. In addition, the exact nonlinear model supplies the simulation's plant dynamics. As discussed earlier, the linearized equations that describe the satellite relative motion are known as Hill's equations (or Clohessy–Wiltshire equations[8]):

$$\begin{aligned}\ddot{x} - 2\omega\dot{y} - 3\omega^2 x = u_x + d_x, \qquad \ddot{y} + 2\omega\dot{x} = u_y + d_y \\ \ddot{z} + \omega^2 z = u_z + d_z\end{aligned} \tag{31}$$

where x, y, and z are member satellite positions relative to a leader satellite in a circular orbit: x is in the radial direction from the Earth, y is in leader satellite's tangential velocity direction, and z completes a right-hand coordinate system. The leader satellite angular velocity ω around the Earth (also known as the mean motion) is described

$$\omega = \sqrt{\mu/R^3} \tag{32}$$

where μ is the Earth's gravitational constant and R is the radius of the leader satellite's circular orbit. The control variables (u_x, u_y, and u_z) and the disturbances (d_x, d_y, and d_z) are net specific forces applied to the two-satellite system. The disturbances in Eq. (31) include the net effects of unmodeled dynamics, net gravitational perturbations, net atmospheric drag, net solar radiation pressure, and net third-body effects.

Our control problem is to design a control system for each member satellite within the formation that drive the satellites toward a desired trajectory relative to the formation leader. In linear approximations that yield Hill's equations, all relative motion closed paths are ellipses. The desired trajectory is a sustainable, natural, elliptic relative motion path when both satellites are free of control forces and unwanted perturbations.[9] A sustainable elliptic path maintains its relative position with respect to the leader. In explicit form, the family of sustainable elliptic paths is given by

$$\hat{x}(t) = r\sin(\omega t + \theta), \qquad \hat{y}(t) = 2r\cos(\omega t + \theta)$$
$$\hat{z}(t) = mr\sin(\omega t + \theta) + 2nr\cos(\omega t + \theta) \tag{33}$$

where r determines the relative motion path size around the leader, θ characterizes the member satellite position on the relative motion path, and m and n describe the plane slope in which the relative motion path resides.[9] Reference trajectories are chosen from this elliptic path family, which is a subset of the force free Hill's equation general solution. An arbitrary initial condition may give rise to an unsustainable closed path, which can not sustain a formation. Because Eq. (33) includes all sustainable paths of relative motion, it includes J_2 invariant trajectories, provided that the leader satellite is in a circular (or near circular) orbit.

Because of fuel limitations, we cannot expect the controlled satellite transient to settle in a short-order time constant. The transient response should have a time constant commensurate with the leader satellite mean motion. Therefore, we shall scale the time axis so that, within each scaled time unit, the leader satellite sweeps a 1-rad arc around the Earth, regardless of the satellite altitude. We introduce a new time variable, $\tau = \omega t$. When $\tau = 1$, the leader sweeps a 1-rad arc around the Earth. Since $\mathrm{d}x/\mathrm{d}t = \omega(\mathrm{d}x/\mathrm{d}\tau)$ and $\mathrm{d}^2x/\mathrm{d}t^2 = \omega^2(\mathrm{d}^2x/\mathrm{d}\tau^2)$, Hill's equations (31) take the following form after the independent variable t is changed to τ:

$$\ddot{x} - 2\dot{y} - 3x = u_x/\omega^2 + d_x/\omega^2$$
$$\ddot{y} + 2\dot{x} = u_y/\omega^2 + d_y/\omega^2, \qquad \ddot{z} + z = u_z/\omega^2 + d_z/\omega^2 \tag{34}$$

For convenience, we are renaming the control inputs, disturbances, and derivates so that they are with respect to τ instead of t. Note that, in Eqs. (31) and (34), the control forces u_x, u_y, and u_z and disturbances d_x, d_y, and d_z are net specific forces applied to the leader–member satellite system. Net refers to the difference between the specific forces applied to the member satellite and those applied to the leader satellite. Specific forces are applied to each unit mass of the respective satellites. Specific forces are actually accelerations. In close formations, the net disturbances are greatly reduced from the absolute amount that is exerted on the member satellite. Now, if we redefine the specific force as the force per unit mass per mean motion squared, ω^2, then we can rewrite Eq. (34) as

$$\ddot{x} - 2\dot{y} - 3x = u_x + d_x, \qquad \ddot{y} + 2\dot{x} = u_y + d_y$$
$$\ddot{z} + z = u_z + d_z \tag{35}$$

Every term in Eq. (35) has a length dimension. One must add the specific control forces (per unit mass of the leader) acting on the leader satellite to the net specific control forces in the right-hand side of Eq. (35) to obtain the specific control forces acting on the member satellite. The same applies to the disturbances. To obtain the actual forces exerted on the member satellite, one must multiply the specific control forces by the satellite mass and by the square of the leader satellite's mean motion. Note that the normalized equations (35) are free of satellite parameters. The relationship between the net specific control force and the actual control forces acting on the member satellite are

$$u_x = u_{fx} - u_{lx}, \qquad u_{lx} = 1/m_l\omega^2(u_{lx})_{\text{actual}}$$
$$u_{fx} = 1/m_f\omega^2(u_{fx})_{\text{actual}} \tag{36}$$

where $(u_{fx})_{\text{actual}}$ is the actual force x component exerted on the member satellite, $(u_{lx})_{\text{actual}}$ is the actual force x component exerted on the leader satellite, m_f is the follower satellite mass, m_l is the leader satellite mass, u_{fx} is the specific force x component exerted on the member satellite, and u_{lx} is the x component of the specific force acting on the leader satellite. The same relation holds for the component forces in other axes.

When the time variable is changed to τ for the reference trajectory, Eq. (33) yields

$$\hat{x}(\tau) = r\sin(\tau + \theta), \qquad \hat{y}(\tau) = 2r\cos(\tau + \theta)$$
$$\hat{z}(\tau) = mr\sin(\tau + \theta) + 2nr\cos(\tau + \theta) \tag{37}$$

Equations (35) show that the in-plane (xy-plane) dynamics given by Hill's equations are decoupled from the cross-track (z-axis) dynamics. We can now write the in-plane dynamic state equations in second-order vector form as

$$\dot{\boldsymbol{x}}_1 = \boldsymbol{x}_2, \qquad \dot{\boldsymbol{x}}_2 = \boldsymbol{A}_1\boldsymbol{x}_1 + \boldsymbol{A}_2\boldsymbol{x}_2 + \boldsymbol{u}_{xy} + \boldsymbol{d}_{xy}, \qquad \boldsymbol{y}_1 = \boldsymbol{x}_1 \tag{38}$$

where the state, output, control, and disturbance vectors are

$$\boldsymbol{x}_1 = \begin{bmatrix} x \\ y \end{bmatrix}, \qquad \boldsymbol{x}_2 = \begin{bmatrix} \dot{x} \\ \dot{y} \end{bmatrix}, \qquad \boldsymbol{u}_{xy} = \begin{bmatrix} u_x \\ u_y \end{bmatrix}, \qquad \boldsymbol{d}_{xy} = \begin{bmatrix} d_x \\ d_y \end{bmatrix} \tag{39}$$

where x and y are scalars denoting the member satellite vertical and tangential coordinates relative to the leader, u_x and u_y are the corresponding net specific control force components on the member satellite, and d_x and d_y are net specific disturbances on the member satellite. To distinguish between vectors and scalars, we now use boldface lower case letters to denote vectors. The state matrices in Eq. (38) are given by

$$A_1 = \begin{bmatrix} 3 & 0 \\ 0 & 0 \end{bmatrix}, \qquad A_2 = \begin{bmatrix} 0 & 2 \\ -2 & 0 \end{bmatrix} \tag{40}$$

The member satellite cross-track dynamics relative to its leader are given by

$$\dot{\xi}_1 = \xi_2, \qquad \dot{\xi}_2 = -\xi_1 + u_z + d_z, \qquad z = \xi_1 \tag{41}$$

where z is the member satellite cross-track coordinate relative to the leader, u_z is the corresponding net specific force component on the member satellite, and d_z is the cross-track net specific disturbance component on the member satellite.

Now, we have two decoupled control problems. For the in-plane dynamics, we design a control policy so that the plant output shown in Eq. (38) tracks the reference trajectory

$$\hat{y}_1(\tau) = \begin{bmatrix} \hat{x}(\tau) \\ \hat{y}(\tau) \end{bmatrix} = \begin{bmatrix} r\sin(\tau + \theta) \\ 2r\cos(\tau + \theta) \end{bmatrix} \tag{42}$$

for some given values of r, q, w, m, and n. This reference trajectory is generated by

$$\dot{\hat{\boldsymbol{x}}}_1 = \hat{\boldsymbol{x}}_2, \qquad \dot{\hat{\boldsymbol{x}}}_2 = \boldsymbol{A}_1\hat{\boldsymbol{x}}_1 + \boldsymbol{A}_2\hat{\boldsymbol{x}}_2, \qquad \hat{\boldsymbol{x}}_1(0) = \begin{bmatrix} r\sin(\theta) \\ 2r\cos(\theta) \end{bmatrix}$$
$$\hat{\boldsymbol{x}}_2(0) = \begin{bmatrix} r\cos(\theta) \\ -2r\sin(\theta) \end{bmatrix}, \qquad \hat{\boldsymbol{y}}_1 = \hat{\boldsymbol{x}}_1 \tag{43}$$

Likewise, we design a cross-track control policy so that the plant output in Eq. (41) tracks the reference trajectory

$$\hat{z}(\tau) = mr\sin(\tau + \theta) + 2nr\cos(\tau + \theta) \tag{44}$$

This reference trajectory is generated as follows:

$$\dot{\hat{\xi}}_1 = \hat{\xi}_2, \qquad \dot{\hat{\xi}}_2 = -\hat{\xi}_2$$

$$[\hat{\xi}(0)] = \begin{bmatrix} mr\sin(\theta) + 2nr\cos(\theta) \\ mr\cos(\theta) - 2nr\sin(\theta) \end{bmatrix}, \qquad \hat{z} = \hat{\xi}_1 \quad (45)$$

Modern satellite systems use high-power jets to produce the desired control forces. The jets usually operate in a short pulse sequence. Recall our assumption that pulse magnitudes are not variable, whereas pulse widths are variable. Therefore, we shall use the discontinuous sliding mode control without continuous components. We shall incorporate a sliding plane boundary layer that prevents chattering as described in Eq. (28). In this control law, we need to compute $B^{*T}(x, t)$ and $\sigma(e)$. We also need $B^{*-1}(x, t)$ and $\tilde{\boldsymbol{u}}(t)$ to determine the minimum control variable magnitude.

For the linear systems model, we can separately design control laws for in-plane and cross-track dynamics. Because the disturbances are in the form of matching uncertainties, we ignore the disturbances in this design, and allow the inherent sliding mode robustness to maintain system stability. First, we shall determine the plant relative degree. From Eq. (38), we obtain

$$\ddot{y}_1(\tau) = a^*_{xy}(x, \tau) + B^*_{xy}(x, \tau)[u(\tau) + d(\tau)] \quad (46)$$

where

$$a^*_{xy}(x, \tau) = A_1x_1 + A_2x_2 = \begin{bmatrix} 3x + 2\dot{y} \\ -2\dot{x} \end{bmatrix}$$

$$B^*_{xy}(x, \tau) = \begin{bmatrix} 1 & 0 \\ 0 & 1 \end{bmatrix} \quad (47)$$

From Eq. (47), the in-plane dynamic relative degree is (2,2). For the cross-track dynamic in Eq. (41), we have

$$\ddot{z} = a^*_z(\xi, \tau) + B^*_z(\xi, \tau)(u_z + d) \quad (48)$$

where

$$a^*_z(\xi, \tau) = -\xi_1, \qquad B^*_z(\xi, \tau) = 1 \quad (49)$$

Therefore, the cross-track dynamics relative degree is 2.

B. Effects of Disturbances and Perturbations

Sliding mode control is inherently robust. The trajectories on the sliding surface exhibit invariance in the presence of bounded unknown, matched uncertainties and disturbances.[10,11] Matched uncertainties or disturbances reside in the range of control distribution matrix. In other words, if matched uncertainties or disturbances are known, control variables can counteract against them. In the satellite formation control problem, microsatellites are modeled as point masses. The atmospheric drag, Earth gravitational perturbations, third-body effects, and unmodeled dynamics all result in matched perturbations within the satellite model.

Sliding mode control is intrinsically robust against matched uncertainties. The control is always driving the system toward the sliding plane. If the disturbance d is acting in the same direction as the control u, then d reinforces u and drives the system faster toward the sliding plane. Because control magnitude does not adjust, control is required for a shorter duration in this direction. The performance is actually improved. Now suppose the disturbance acts in the opposite direction as the control. The system is driven toward the sliding plane slower. Control is required for a longer duration to enable the system to reach the sliding plane. In this fashion, the control automatically adjusts its pulse width. When the system is on the sliding plane, the error dynamics are determined by the sliding plane parameters.

The most significant orbiting perturbation is J_2 effect. The J_2 effect accounts for Earth oblateness, and the J_3 effect accounts for the Earth's polar bulges. Hill's equations (31) and (35) do not account for the nonspherical Earth effects, nor the nonlinear dynamics Eq. (58). The J_2 effect is nearly two orders of magnitude more pronounced than J_3. These gravity perturbations will move an uncontrolled satellite from its nominal orbit. The disturbances in our model are net specific disturbances. In close formations, the net disturbances are significantly reduced from total disturbances, but are still consequential. Sabol et al.[2] simulated a two-satellite formation where the J_2 effect gradually disperses the formation. Solar radiation pressure and tesseral resonance are periodic and will gradually wear out the formation, causing its members to disperse relative to each other. In tracking control, the effects of solar radiation pressure and tesseral resonance are also countered by control thrusts.

C. Third-Order Sliding Plane Design

We choose a sliding plane in the form of Eq. (11). The error function rapidly approaches zero when the system state is on that plane. The sliding plane produces a proportional-plus-integral-plus-derivative equivalent control on the feedback-linearized plant. Applying the satellite system relative degrees to Eq. (11) yields the sliding planes for both the in-plane dynamics and the cross-track dynamics in the form

$$\sigma(e) = \frac{\mathrm{d}}{\mathrm{d}\tau}e(\tau) + K_1e(\tau) + K_0e_s(\tau) + K_se_{ss}(\tau) \quad (50)$$

We shall design the control system for the error signal in each coordinate to have the same transient characteristics. The error dynamics have the following three poles:

$$p_1 = -0.15, \qquad p_2 = 0.05\left(-1 \pm j\sqrt{3}\right) \quad (51)$$

We are placing the real part of the dominant poles at -0.05 with a 0.5 damping ratio. This yields a time constant of $\tau = 20$. Therefore, the settling time is approximately $\tau_{\text{settling}} = 80$. Because the normalized time unit is a radian, the leader sweeps approximately 13 orbits around the Earth before the error transient settles. Therefore,

$$(s - p_1)(s - p_2)(s - p_3) = s^3 + 0.25s^2 + 0.025s + 0.0015 \quad (52)$$

Comparing Eq. (50) with Eq. (52) gives

$$K_1 = 0.25I, \qquad K_0 = 0.025I, \qquad K_s = 0.0015I$$

The error dynamics characteristic polynomial Eq. (52) is third order. The discontinuous sliding mode control laws are obtained by substituting Eqs. (50) and (53) into Eq. (28):

$$u_i(\tau) = \begin{cases} \rho_i, & \text{if } \delta_i < \dot{e}_i(\tau) + 0.25e_i(\tau) + 0.025e_{si}(\tau) \\ & \quad + 0.0015e_{ssi}(\tau) \\ 0, & \text{if } -\delta_i \le \dot{e}_i(\tau) + 0.25e_i(\tau) + 0.025e_{si}(\tau) \\ & \quad + 0.0015e_{ssi}(\tau) \le \delta_i \\ -\rho_i, & \text{if } \dot{e}_i(\tau) + 0.25e_i(\tau) + 0.025e_{si}(\tau) \\ & \quad + 0.0015e_{ssi}(\tau) < -\delta_i \end{cases}$$

$$\rho_i > \max|\tilde{u}_i(t)|, \qquad i = x, y, z \quad (53)$$

where the control signal magnitude has a lower bound that is determined by simulation.

A closed-loop system block diagram that implements the sliding mode control law for the in-plane dynamics [Eq. (53)] is given in Fig. 1a. Differentiators are not needed, provided that the system states are measurable. Figure 1b shows the closed-loop sliding mode control block diagram for the cross-track dynamics. In both Figs. 1a and 1b, the controllers are described by Eq. (53).

D. Second-Order Sliding Plane Design

Dropping the double integral term in the right-hand side of Eq. (50) gives the second-order sliding plane equation for both the in-plane and cross-track dynamics:

$$\sigma(e) = \frac{\mathrm{d}}{\mathrm{d}\tau}e(\tau) + K_1e(\tau) + K_0e_s(\tau) \quad (54)$$

We will select the two complex poles in Eq. (51) as the characteristic roots of Eq. (54). Thus,

$$p_1 = 0.05\left(-1 \pm j\sqrt{3}\right) \quad (55)$$

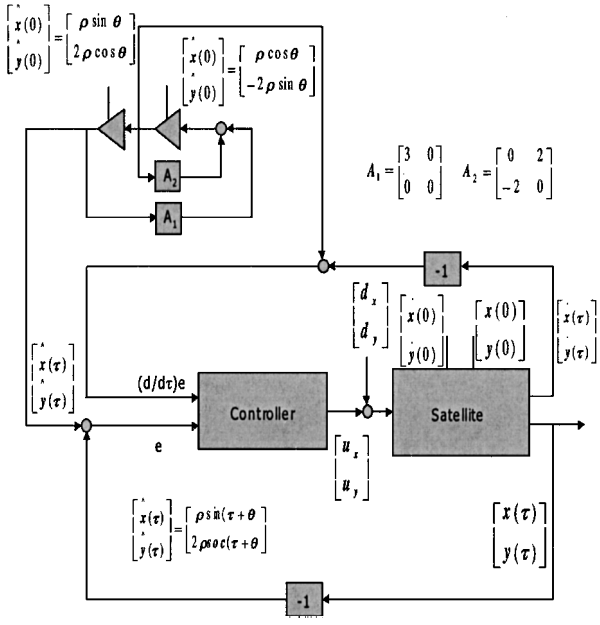

a) In-plane tracking control

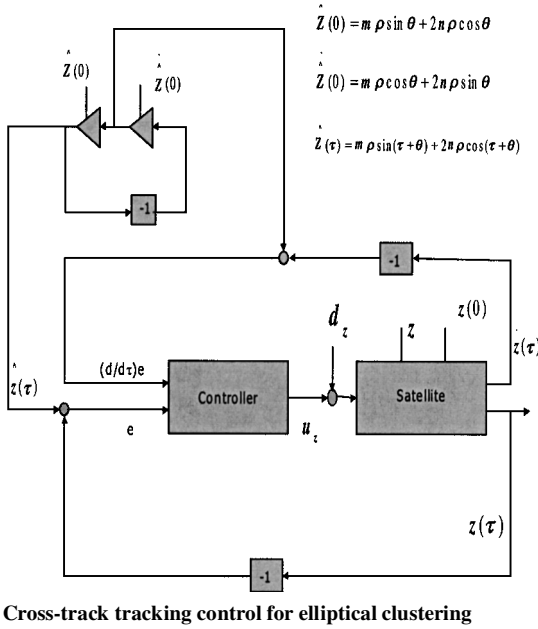

b) Cross-track tracking control for elliptical clustering

Fig. 1 Generalized closed-loop system for satellite formation.

and

$$(s - p_1)(s - p_2) = s^2 + 0.1s + 0.01 \tag{56}$$

Comparison of Eq. (54) with Eq. (56) gives

$$K_1 = 0.1I, \qquad K_0 = 0.01I$$

We shall design the control system to have the same transient characteristics as in the third-order case discussed in Sec. III.C. The discontinuous sliding mode control laws with a second-order sliding plane are obtained by substituting Eqs. (54) and (57) into Eq. (58),

$$u_i(\tau) = \begin{cases} \rho_i, & \text{if} \quad \delta_i < \dot{e}_i(\tau) + 0.1e_i(\tau) + 0.01e_{si}(\tau) \\ 0, & \text{if} \quad -\delta_i \le \dot{e}_i(\tau) + 0.1e_i(\tau) + 0.01e_{si}(\tau) \le \delta_i \\ -\rho_i, & \text{if} \quad \dot{e}_i(\tau) + 0.1e_i(\tau) + 0.01e_{si}(\tau) < -\delta_i \end{cases}$$

$$\rho_i > \max|\tilde{u}_i(t)|, \qquad i = x, y, z \tag{57}$$

where the control signmal magnitude has a lower bound that is determined by simulation. In the simulation runs discussed in Sec. IV, we will readjust K_1 and K_2 to search for sliding plane that require minimal fuel consumption.

E. Sliding Mode Control for the Nonlinear Plant

Under the assumptions that the Earth is a perfect sphere and the leader satellite is in a circular orbit, the normalized, nonlinear model is described by

$$\ddot{x} - 2\dot{y} + (R + x)[g(x, y, z, R) - 1] = u_x + d_x$$

$$\ddot{y} + 2\dot{x} + y[g(x, y, z, R) - 1] = u_y + d_y$$

$$\ddot{z} + zg(x, y, z, R) = u_z + d_z \tag{58}$$

where

$$g(x, y, z, R) = \{[(R + x)^2 + (y^2 + z^2)^2]/R^2\}^{-\frac{3}{2}} \tag{59}$$

Hill's equation (35) is the linear approximation of this model,

$$\boldsymbol{y} = \begin{bmatrix} x \\ y \\ z \end{bmatrix}, \qquad f_x(\boldsymbol{y}) = (R + x)[1 - g(x, y, z, R)] - 3x$$

$$f_y(\boldsymbol{y}) = y[1 - g(x, y, z, R)],$$

$$f_z(\boldsymbol{y}) = z[1 - g(x, y, z, R)] \tag{60}$$

Then, we rewrite Eq. (58) into the following form:

$$\ddot{x} - 2\dot{y} - 3x - f_x(\boldsymbol{y}) = u_x + d_x$$

$$\ddot{y} + 2\dot{x} - f_y(\boldsymbol{y}) = u_y + d_y, \qquad \ddot{z} - z - f_z(\boldsymbol{y}) = u_z + d_z \tag{61}$$

Using the satellite dynamics nonlinear model described in Eq. (51) is a step beyond the linear Hill's model. The reference trajectory is a periodic relative motion path that satisfies the homogeneous equations in Eq. (51) (when $\boldsymbol{u}$ and $\boldsymbol{d}$ are both set equal to zero). However, the general solution to the system described in Eq. (51) has not been found. Therefore, we shall improvise by using the initial condition determined from the homogeneous Hill's solution to the homogeneous nonlinear model to generate the reference trajectory numerically. We shall assume that the initial conditions taken from the linear model [Eqs. (42) and (45)] will result in closed-path solutions for the homogeneous nonlinear model of Eq. (51) and shall verify it by simulations. Numerical experiments have shown that the initial conditions that produce a sustainable, elliptic path for the homogeneous model also produce a sustainable elliptic closed path for the homogeneous nonlinear model.[12] A reference trajectory generated from the nonlinear model results in a tracking control that will not fight the nonlinearity on the satellite. Using the nonlinear model as the plant's design model gives a more truthful dynamic than that produced by the linear Hill's equations.

The reference trajectory is generated by the force-free nonlinear model with initial conditions set by the desired trajectory of the linear model (Hill's equations):

$$\ddot{\hat{x}} - 2\dot{\hat{y}} - 3\hat{x} - f_x(\hat{\boldsymbol{y}}) = 0, \qquad \ddot{\hat{y}} + 2\dot{\hat{x}} - f_y(\hat{\boldsymbol{y}}) = 0$$

$$\ddot{\hat{z}} - \hat{z} - f_z(\hat{\boldsymbol{y}}) = 0 \tag{62}$$

The initial conditions are obtained from Eq. (33):

$$\begin{bmatrix} \hat{x}(0) \\ \hat{y}(0) \\ \hat{z}(0) \end{bmatrix} = \begin{bmatrix} r\sin\theta \\ 2r\cos\theta \\ mr\sin\theta + 2nr\cos\theta \end{bmatrix}$$

$$\begin{bmatrix} \dot{\hat{x}}(0) \\ \dot{\hat{y}}(0) \\ \dot{\hat{z}}(0) \end{bmatrix} = \begin{bmatrix} r\cos\theta \\ -2r\sin\theta \\ mr\cos\theta - 2nr\sin\theta \end{bmatrix} \tag{63}$$

It is difficult to find the closed-form solutions of Eqs. (62) and (63), but simulation[4] shows that the solutions appear elliptic.

When comparing Eqs. (61) and (35), the difference between the linear and nonlinear model is a matched perturbation entering the linear model at the same point as the control input. Therefore, one can modify designs created for the linear plant model to incorporate the nonlinear model. One would need to add perturbations $f_x(\boldsymbol{y})$, $f_y(\boldsymbol{y})$, and $f_z(\boldsymbol{y})$ to the corresponding plant input ports and $f_x(\hat{\boldsymbol{y}})$, $f_y(\hat{\boldsymbol{y}})$, and $f_z(\hat{\boldsymbol{y}})$ to the corresponding reference model input ports.

IV. Numerical Simulation

This section summarizes the simulation efforts to control a microsatellite formation using a sliding mode framework. A leader satellite orbits in a low-Earth, open-loop polar orbit while a follower satellite is actively controlled. The control effort discusses design parameters for a fuel minimization objective.

A. Closed-Loop Design Considerations

As described in preceding sections, tracking control requires a desired dynamics model of the satellite relative motion. The sliding mode controller works to minimize the differences between the desired and actual relative motion for each of the Cartesian coordinate directions. For this current research effort, we use linear Hills equations (31) to provide the desired relative motion. An independent sliding mode algorithm is created for each direction. Control thrusts are, therefore, determined and applied independently for each direction.

To account for the discrete nature of the control thrusts, we add a nonlinear block that regulates the control thrust input. In each moving coordinate frame direction, the σ function from Eqs. (50) and (54) monitors the error between desired and actual relative position, relative velocity, and integral of error position. In addition, the third-order sliding mode case (Sec. III.C) incorporates the error position's second integral. The simulation assumes instantaneous sensing of these variables. If $|\sigma|$ is less than some defined threshold, δ_i, where $i = x, y, z$, control inputs are zero. If $|\sigma|$ exceeds δ_i, a constant control force is applied. These thrust levels are adjustable to better simulate the actual thrust magnitude for a given application.

Our simulation incorporates a high-fidelity orbital propogation algorithm written by Princeton Satellite Systems for MATLAB®. This algorithm propagates each satellite independently in the Earth centered inertial reference frame. It permits user-defined levels of disturbances, such as drag, solar impacts, third-body impacts from the moon's gravity, and nonspherical Earth impacts. In addition, the high-fidelity code accepts external force inputs, providing a convenient means to simulate control forces.

We consider the case where satellites orbit the Earth in near polar orbits. The leader satellite is in a circular orbit, while the follower's orbit has some eccentricity to produce the desired relative motion. The leader satellite's starting position has an 800-km altitude, with mean anomaly, longitude of ascending node, and argument of perigee equaling zero. The relative orbit between satellites is circular. The leader exists in the formation center, while the follower satellite attempts to maintain a 1 km radius. Thrust for station keeping is only applied to the follower satellite; the leader satellite orbits the Earth open loop. The control law would also apply if the leader were controlled to the desired track. The simulation includes the Earth oblateness effect. We note that there are negligible differences in tracking the nonlinear Hill's case [Eq. (61)] compared to the linear Hill's case [Eq. (35)].

B. Design Tradeoffs

The sliding mode design incorporates a number of design tradeoffs. In this section, all thrust levels and fuel consumptions, ΔV, are expressed in normalized net specific values as defined in Eq. (35). Note that ΔV is the integral of the specific control forces. The poles associated with the sliding surface are a primary variable when considering the closed-loop design. The sliding surface gives the characteristic equation of the closed-loop response when the equivalent control of the sliding mode is implemented, that is, when the controlled system is on the sliding plane. We initially investigated a second-order sliding surface. The second-order poles are found in the left-hand plane and take the form $-X \pm jY$ (Fig. 2a). We investigated several sliding plane pole locations to analyze their impact on fuel consumption, as measured by the amount of velocity required for stationkeeping, ΔV (Fig. 2b). To formulate a reasonable comparison, we maintained the normalized natural frequency of the characteristic equation at 0.1. This normalized natural frequency unit results by changing the time variable from t to τ in Eq. (31). To minimize the ΔV requirement, the most effective cases correspond to a damping ratio between 0.866 and 0.966. These damping ratios minimize the overshoot of the thrust response. We found that the cases with smaller damping ratio less than 0.5 require additional control energy to maintain an acceptable sliding surface boundary layer δ_i. In addition, larger damping ratios (0.966 or higher) at this natural frequency drive the follower satellite toward the desired orbit too aggressively. This overcorrection costs more energy as well.

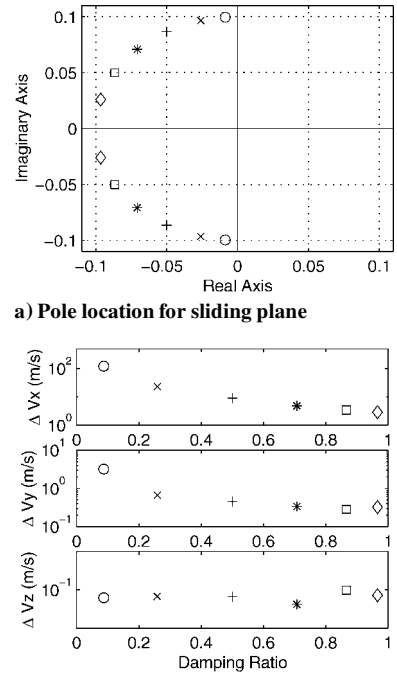

a) Pole location for sliding plane

b) ΔV vs damping ratio

Fig. 2 Damping ratio variation: weekly fuel consumption.

The ΔV consumption is highly dependent on the bandwidth of the sliding plane poles. Consider the case where the characteristic pole is located along the $\zeta = 0.5$ line. We have chosen several bandwidth samples (Fig. 3a). For a given sliding plane boundary layer δ_i and corrective thrust ρ magnitude, some ideal bandwidth is determined. In this case, it occurs around the 1-rad bandwidth (Fig. 3b). If the bandwidth is too high, the control energy tends to knock the satellite back and forth too frequently. In these cases, the disturbance forces actually cause minimal impact on the error in the satellite's relative position (Fig. 4). For this high bandwidth case (with poles represented as a △ in Fig. 3), the compensator poles are designed to cause the satellite to reach its correct position in a half revolution around the Earth (half of the 100.71 min for this low Earth orbit). Conversely, if the bandwidth is too low, the satellites require a long settling time. As shown in Fig. 4, the satellite is lightly tapped to correct the orbit. The low bandwidth response can require an excessive amount of control energy over the long run. This case corresponds to the pole represented by ○ in Fig. 3.

Another major variable that impacts the desirability of the sliding mode pole location is the thrust magnitude. Recall that the high-fidelity simulation allows direct acceleration thrust insertions into the model. Figure 5 indicates the impact of thrust level for a typical medium bandwidth and moderate damping ratio (where $\zeta = 0.5$). One can achieve improved performance by increasing the corrective thrust level for a given threshold level to a point. Increasing the thrust levels beyond this point overcompensates, resulting in wasted energy from the tighter position error. The solid line in Fig. 6 shows the tighter trajectory tracking. Thrust magnitude decreases also require

excessive ΔV requirements and create looser positional error. This position error is shown by the dash–dot line in Fig. 6.

One can draw similar conclusions about the threshold values that trigger the corrective thrusts. Varying δ_i produces a parabolic ΔV curve (Fig. 7). Given some selection for control parameters such as damping ratio and natural frequency, we can formulate some rule of thumb that relates the triggering threshold for the prescribed thrust magnitude. Excessive drift usually requires too much corrective thrust to make loose tolerances feasible. On the other hand, excessively tight tolerances cause overcompensation because the satellite bounces between threshold extremes.

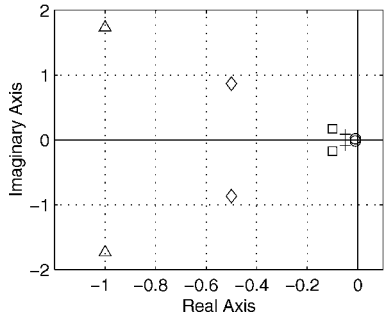

a) Pole location for sliding plane

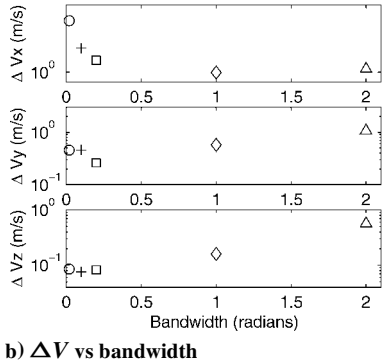

b) ΔV vs bandwidth

Fig. 3 Bandwidth variation: weekly fuel consumption.

C. Initial Condition Offset

The satellite formation control work discussed thus far primarily addresses the station keeping function. This effort requires a control law to counter routine perturbations based on the imperfect orbiting conditions. The second major objective for the control function focuses on relatively large-scale corrections to an orbit. Typical examples for this control requirement exist when there is a need to rearrange the formation or after the initial satellite deployment. In other words, two sets of control laws are required for each satellite. One can chose to construct each of these control algorithms in a similar framework, such as sliding mode. A switching mechanism will determine which control algorithm is used at a given time, depending on the immediate need.

We consider an initial deployment positional correction example. This scenario simulates when the satellites are initially placed into space and not at the correct location with the correct velocity components. The follower satellite is in a circular relative formation with a 1.49 km radius. The sliding mode design is overdamped to enhance large maneuver efficiency, that is, the sliding mode design has two real poles. Figure 8 shows an initial satellite cluster deployment. As one can see, the circular orbit is quickly formed with the given low-thrust level used later for control. In this particular case, a ΔV of 2.29 m/s is consumed to correct the relative formation in 0.42 orbits. The sliding mode control design works well at bringing the satellite formation into the desired circular orbit.

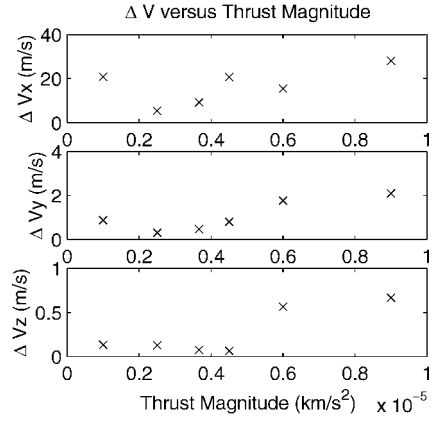

Fig. 5 Weekly velocity requirements: thrust magnitude variation.

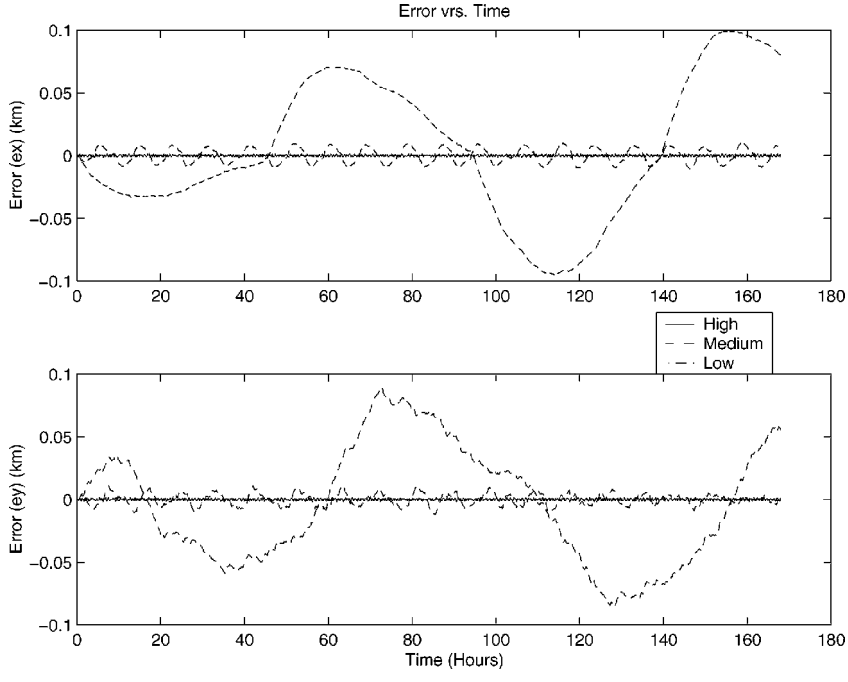

Fig. 4 Different bandwidths impact on position error: maintaining 0.5 damping ratio.

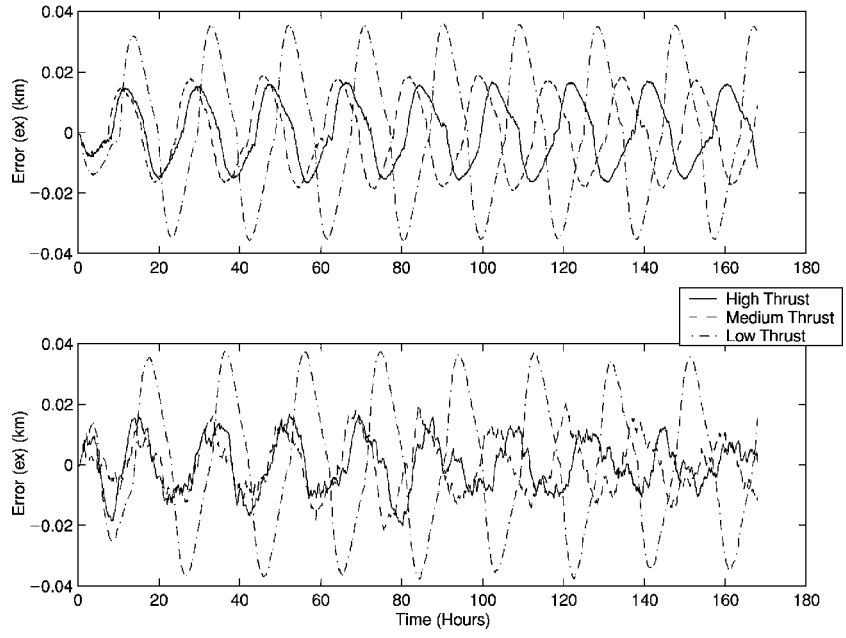

Fig. 6 Thrust variation examples: maintaining 0.5 damping ratio and moderate bandwidth.

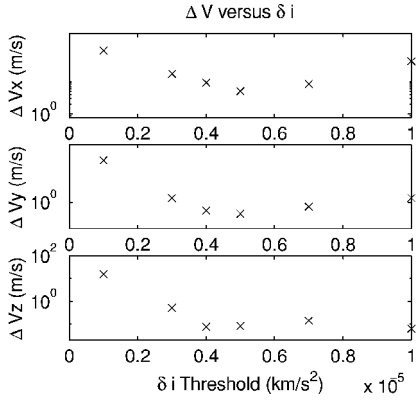

Fig. 7 Weekly velocity requirements: varying threshold to trigger thrusting.

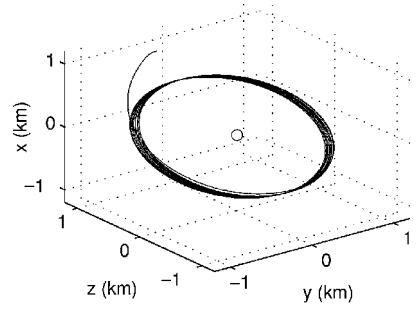

Fig. 8 Relative position error for large magnitude maneuvers.

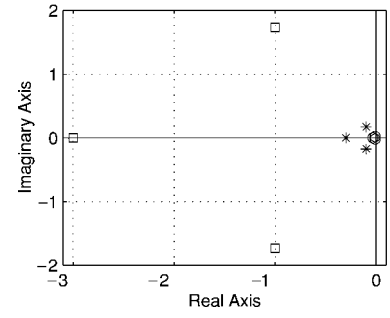

a) Pole location for sliding plane

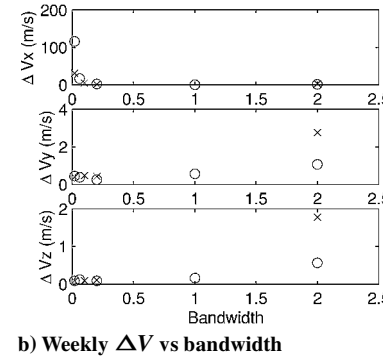

b) Weekly ΔV vs bandwidth

Fig. 9 Bandwidth variation: third order (×) and second order (○).

D. Third-Order Compensator Design

We also considered a third-order sliding plane design. This compensation strategy incorporates one additional term into the σ function (a relative position error double integral). Compare the sliding mode pole placements between Figs. 9a and 3a. The dominant complex correspond in these two cases. Figure 9b shows the comparative results for the same dominant poles. For the lower bandwidth poles with a damping ratio of 0.5, the third-order design improves the ΔV performance. Conversely, the third-order case decreases performance for higher bandwidth cases. For the best cases, adding a third pole to the sliding plane produces a negligible impact.

E. Nominal Baseline Design Under High-Order Perturbations

The sliding mode design is robust to various perturbations. The methodology only requires a tracking signal that indicates what the desired relative position and velocity vectors are. Recall that we track a trajectory derived from the linear Hill's equation as our desired dynamics. We compare two orbiting dynamic models: the high-fidelity simulation with J_2 only and the all perturbative force options available in the high-fidelity simulation including higher-order Earth gravitational effects, atmospheric drag, solar radiation, solar disturbances, and lunar and solar gravity.

We found that as the bandwidth of the closed-loop system increases, the differences in perturbative forces becomes negligible in terms of fuel usage compared to the J_2 case discussed earlier. This is because more power is used to drive the system toward the sliding mode and disturbance affects are attenuated more effectively. The disturbance effects are more noticeable at lower bandwidth designs. There are negligible closed-loop response differences between the

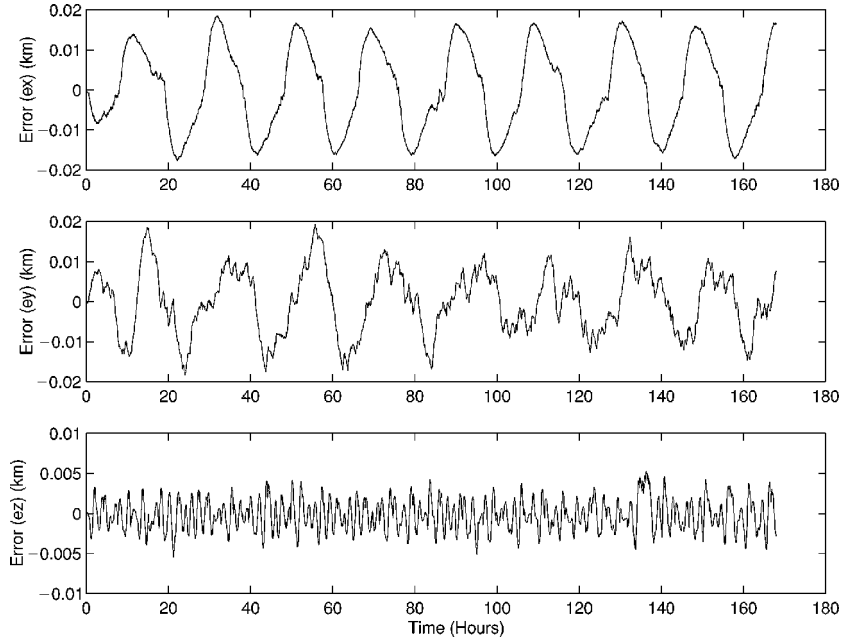

Numerous perturbation case

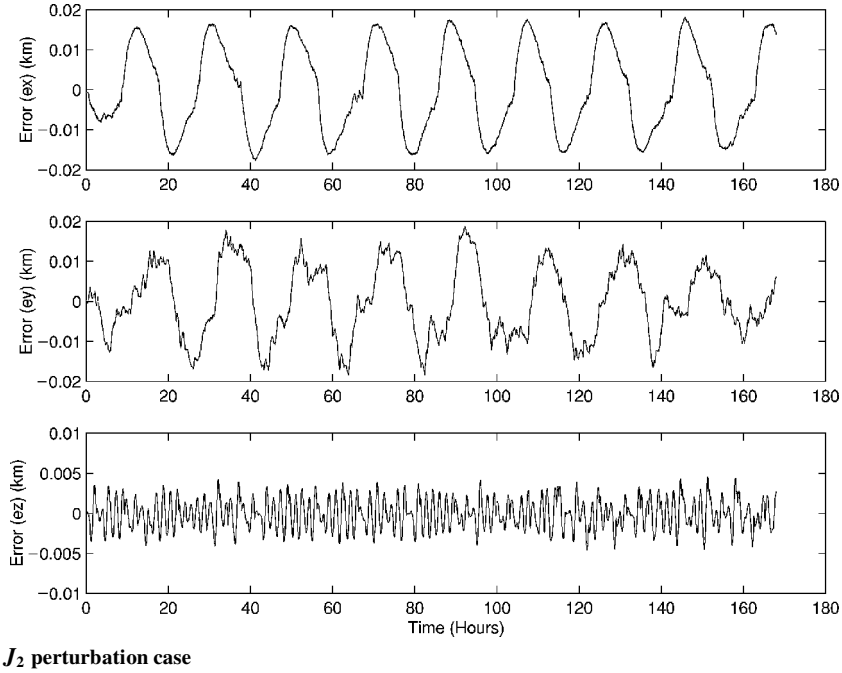

J_2 perturbation case

Fig. 10 Nominal design example.

J_2-only disturbance case and the numerous perturbation case. In fact, for a simulation with a 1-week duration, the J_2-only case requries approximately the same ΔV as the extensive perturbation case, to within 1%. Figure 10 shows the similar position error for these cases. This supports the conclusion that J_2 is the dominant perturbation at this orbit trajectory.

V. Conclusions

In this paper, a tracking control design using sliding mode techniques is derived to control a desired satellite formation. The sliding mode control technique provided a viable approach to the design of a control law to control the position of a follower satellite relative to a leader. Numerical studies provided insight into the selection of design parameters for the sliding mode control law. The most effective equivalent damping ratio of the sliding plane was found to be between 0.8 and 1.0, in this case minimizing the overshoot of the thrust responses. Smaller damping ratios require additional control energy whereas large ones drive the satellite too agressively. In addition, the desired bandwidth of the desired plane was found to be in the 1 rad/s range. This value provides an acceptable tradeoff between control energy and tracking accuracy.

References

[1] Kapila, V., Sparks, A. G., Buffington, J. M., and Yan, Q., "Spacecraft Formation Flying: Dynamics and Control," *Journal of Guidance, Control, and Dynamics*, Vol. 23, No. 3, 2000, pp. 561–564.

[2] Sabol, C., Burns, R., and McLaughlin, C., "Formation Flying Design and Evolutions," *Journal of Spacecraft and Rockets*, Vol. 38, No. 2, 2001, pp. 270–278.

[3] Schaub, H., Vadali, S. R., Junkins, J. L., and Alfriend, K. T., "Space Craft Formation Flying Control Using Mean Orbit Elements," AAS Astrodynamic Conf., NASA Goddard Space Flight Center, Greenbelt, MD, 1999.

[4] Schaub, H., and Alfriend, K. T., "J_2 Invariant Reference Orbits for Space Craft Formations," Flight Mechanics Symposium, NASA Goddard Space Flight Center, Greenbelt, MD, May 1999.

[5]Singh, S. N., "Asymptotically Decoupled Discontinuous Control of Systems and Nonlinear Aircraft Maneuver," *IEEE Transactions on Aerospace and Electronic Systems*, Vol. 25, No. 3, 1989, pp. 380–390.

[6]De Carlo, R. A., Zak, S. H., and Mathews, G. P., "Variable Structure Control of Nonlinear Multivariable Systems: A Tutorial," *Proceedings of the IEEE*, Vol. 76, No. 3, 1988, pp. 212–232.

[7]Bartolini, G., and Pydynowski, P., "An Improved Chattering Free VSC Scheme for Uncertain Dynamical Systems," *IEEE Transactions on Automatic Control*, Vol. 41, No. 11, 1998, pp. 1220–1246.

[8]Clohessy, W. H., and Wiltshire, R. H., "Terminal Guidance System for Satellite Rendezvous," *Journal of the Aerospace Sciences*, Vol. 27, No. 6, 1960, pp. 653–658.

[9]Yeh, H. H., and Sparks, A., "Geometry and Control of Satellite Formations," American Control Conf., June 2000.

[10]Slotine, J. J., and Li, W., *Applied Nonlinear Control*, Prentice–Hall, Upper Saddle River, NJ, 1991, pp. 62–101.

[11]Drazenovic, B., "The Invariant Conditions in Variable Structure Systems," *Automatica*, Vol. 5, No. 3, 1969, pp. 287–295.

[12]de Queiroz, M. S., Kapila, V., and Yan, Q., "Adaptive Nonlinear Control of Multiple Spacecraft Formation Flying," *Journal of Guidance, Control, and Dynamics*, Vol. 23, No. 3, 2000, pp. 385–391.